Domain within the helicase subunit Mcm4 integrates multiple kinase signals to control DNA replication initiation and fork progression

Yi-Jun Sheu[a], Justin B. Kinney[a], Armelle Lengronne[b], Philippe Pasero[b], and Bruce Stillman[a,1]

[a]Cold Spring Harbor Laboratory, Cold Spring Harbor, NY 11724; and [b]Institute of Human Genetics, Centre National de la Recherche Scientifique, Unité Propre de Recherche 1142, 34396 Montpellier, France

Eukaryotic DNA synthesis initiates from multiple replication origins and progresses through bidirectional replication forks to ensure efficient duplication of the genome. Temporal control of initiation from origins and regulation of replication fork functions are important aspects for maintaining genome stability. Multiple kinase-signaling pathways are involved in these processes. The Dbf4-dependent Cdc7 kinase (DDK), cyclin-dependent kinase (CDK), and Mec1, the yeast Ataxia telangiectasia mutated/Ataxia telangiectasia mutated Rad3-related checkpoint regulator, all target the structurally disordered N-terminal serine/threonine-rich domain (NSD) of mini-chromosome maintenance subunit 4 (Mcm4), a subunit of the mini-chromosome maintenance (MCM) replicative helicase complex. Using whole-genome replication profile analysis and single-molecule DNA fiber analysis, we show that under replication stress the temporal pattern of origin activation and DNA replication fork progression are altered in cells with mutations within two separate segments of the Mcm4 NSD. The proximal segment of the NSD residing next to the DDK-docking domain mediates repression of late-origin firing by checkpoint signals because in its absence late origins become active despite an elevated DNA damage-checkpoint response. In contrast, the distal segment of the NSD at the N terminus plays no role in the temporal pattern of origin firing but has a strong influence on replication fork progression and on checkpoint signaling. Both fork progression and checkpoint response are regulated by the phosphorylation of the canonical CDK sites at the distal NSD. Together, our data suggest that the eukaryotic MCM helicase contains an intrinsic regulatory domain that integrates multiple signals to coordinate origin activation and replication fork progression under stress conditions.

DNA helicase | MCM2–7 | Cdc7-Dbf4 kinase

Eukaryotic DNA replication initiates from multiple replication origins within each chromosome to duplicate the large genome efficiently. To ensure DNA synthesis occurs once and only once across the genome, cells adopt a two-step process to activate replication origins during two separate stages of the cell-division cycle. The first step is licensing of replication origins, which occurs only when cyclin-dependent kinase (CDK) activity is low. In *Saccharomyces cerevisiae*, origins of DNA replication are licensed in G1 by the formation of a prereplicative complex (pre-RC). The process begins with the origin recognition complex binding to replication origins and recruiting the licensing factor Cdc6, which facilitates loading of the Cdt1-bound mini-chromosome maintenance (MCM) complex composed of Mcm2–Mcm7 (Mcm2–7). The hexameric Mcm2–7 is the core of the replicative helicase that unwinds DNA during replication. Within the pre-RC Mcm2–7 is loaded as an inactive double hexamer. The next step, activation of licensed origins (origin firing), occurs throughout the S phase and requires the continuous presence of two kinases, the S phase CDKs and the Dbf4-dependent Cdc7 kinase (DDK). CDK phosphorylates Sld2 and Sld3 to allow their binding to Dpb11 (1, 2), facilitating recruitment of Cdc45 and GINS (composed of protein subunits Sld5, Psf1, Psf2 and Psf3; Go,

Ichi, Nii, and San stand for five, one, two, and three in Japanese, respectively) to Mcm2–7 to create an active helicase. DDK phosphorylates Mcm2–7 and blocks an intrinsic initiation inhibitory activity residing in the N terminus of the Mcm4 subunit (3). The concerted action of these S-phase kinases transforms the inactive Mcm2–7 double hexamer into the active helicase complex composed of Cdc45, Mcm2-7, and GINS (the CMG complex) (4–6). Upon initiation, DNA polymerases and other components of the replication machinery are recruited to form replisomes and establish replication forks, where DNA synthesis ensues.

Kinase-signaling pathways target various components of the replication machinery. Both CDK and DDK target replication proteins in addition to their essential targets described above. Furthermore, Ataxia telangiectasia mutated/Ataxia telangiectasia mutated Rad3-related (ATM/ATR) signaling targets components of the CMG helicase complex under replication stress (7–10). In the yeast *S. cerevisiae*, DNA damage activates the checkpoint kinase Rad53, which phosphorylates both Sld3 and Dbf4 to inhibit late origin firing (11, 12). The yeast ATM/ATR homolog Mec1 also targets Mcm4 (13). The stress-activated protein kinase Hog1 targets an auxiliary replisome component Mrc1 to regulate both origin firing and fork progression (14). Although we now have a better understanding of the essential functions of protein kinases in controlling the initiation of replication, we do not completely understand how the separate kinase signaling pathways are coordinated to regulate both initiation and replication fork progression.

Significance

During each cell-division cycle, eukaryotic cells initiate DNA synthesis from multiple replication origins on chromosomes to duplicate the entire genome once and only once. Spatial and temporal control of initiation and subsequent DNA synthesis at replication forks is important for maintaining genome integrity. Here we present a comprehensive analysis of patterns of origin activation, replication fork progression, and checkpoint responses in cells under replication stress. Our studies showed that a domain intrinsic to the replicative helicase, which unwinds DNA during replication, integrates multiple kinase-signaling pathways to control various aspects of the genome duplication process. Our work suggests a mechanism by which eukaryotic cells modulate the pattern of replication in response to environmental conditions through the replicative helicase.

The structurally disordered N-terminal serine/threonine-rich domain (NSD) of Mcm4 is a target of multiple kinases, including DDK, CDK, and Mec1 (3, 13, 15, 16). Within this region we have identified two functionally distinct domains that exert different functions and are regulated by different kinase systems even though they overlap extensively in primary amino acid sequences. The segment of the Mcm4 NSD proximal to the DDK-docking domain (DDD) (15), and hence termed "proximal NSD," blocks initiation until it is phosphorylated by DDK. In contrast, the distal segment of the NSD at the N terminus, away from the DDD, is targeted by additional kinases and contributes positively to promote S-phase progression. In this study we present a comprehensive analysis of the pattern of origin activation, replication fork progression, and the checkpoint response in cells under replication stress caused by the inhibition of ribonucleotide reductase (RNR). We show that the distal and proximal NSD segments contribute differently to origin activation and DNA replication fork progression. Furthermore, they exert opposing effects on checkpoint signaling under replication stress. All these effects are regulated by phosphorylation. We suggest that the Mcm4 NSD, a regulatory domain intrinsic to the replicative helicase, mediates the control of multiple aspects of DNA replication. Our data reveal a sophisticated mechanism to fine-tune S-phase progression in response to changing environments.

Results

Analysis of the Whole-Genome Replication Profile. To gain a genome-wide view of patterns of origin activation and replication fork progression, we developed a procedure to isolate and analyze newly synthesized DNA from synchronized yeast cell culture by combining the azide-alkyne Huisgen cycloaddition reaction (the "Click" reaction) and high-throughput sequencing (*SI Materials and Methods*). We verified that yeast cells harboring a BrdU-Inc cassette (17) were able to incorporate 5-ethynyl-2'-deoxyuridine (EdU) (18) as well as BrdU. Exponentially growing yeast cells were arrested in G1 using α-factor and were released into fresh medium containing hydroxyurea (HU), EdU, and pronase E to degrade remaining α-factor. Cells were collected 90 min or 180 min after release. Genomic DNA prepared from these cells was fragmented and barcoded. To capture the newly synthesized DNA incorporated with EdU, biotin was coupled to EdU-DNA using Click chemistry, and the biotinylated EdU-DNA samples were isolated using streptavidin beads. These beads did not pull down unlabeled genomic DNA or EdU-DNA without biotinylation. The purified DNA then was examined by high-throughput DNA sequencing. The sequence reads at each genomic locus collectively produced an abundance profile of newly synthesized DNA across the genome. In the 90-min sample, the center of each peak in the profile coincided with annotated origins in the DNA Replication Origin Database (OriDB) (Fig. S1) (19). Thus, the profile provided a picture of the relative frequency of each origin firing within the population of cells and of the distances of bidirectional replication from each origin. DNA synthesis spread further from the origins at 180 min (Fig. S1). The 90-min time point was more informative for analysis of origin firing and fork progression because at 180 min many adjacent peaks merged with each other, as is consistent with a previous finding that DNA synthesis continued in HU, albeit at a slower rate (20). We therefore chose the 90-min time point for further experiments.

The replication profiles of the same yeast strain were highly reproducible in different experiments (Fig. S2A), indicating the utility of this protocol. The patterns of DNA replication were analyzed further computationally to measure the observed peak width at the half maximum of the peak height for each origin in the profile (*Computational Analyses of Sequencing Data* in *SI Materials and Methods*). The observed peak width was plotted against the peak height (Fig. S2B). From these plots, it is apparent

that the observed width for most of the peaks, and thus the average fork progression from any active origin, was very similar for all origins in the same yeast strain, regardless of the peak height. Furthermore, peak widths for any given strain, and hence the fork progression rate, was highly reproducible in different experiments (Fig. S2C and Table 1).

Proximal NSD Affects Patterns of Origin Activation. The Mcm4 NSD encompasses amino acids 1–174 at the N terminus of the protein (see Fig. 4 below). We have shown previously that the proximal NSD (amino acids 74–174) serves as an intrinsic inhibitor of origin activation (3). In contrast, the distal portion of the NSD (amino acids 2–145) contributes positively to promote S-phase progression. To gain insight into which aspect of DNA replication is affected by each NSD segment, we examined the replication profiles of the wild-type cells and various mcm4 mutants containing specific truncations within the NSD and compared their patterns of origin firing. In wild-type cells, only origins that were active early during an unperturbed S phase (early origins) fire in HU (Fig. 1A, profile 1). Interestingly, in contrast to wild-type cells, cells that lacked the proximal NSD ($mcm4^{\Delta74-174}$) not only activated early origins but also fired late origins in HU despite an elevated checkpoint response (see below) (Fig. 1A, profile 3, red arrows). These same late origins did not fire in the $mcm4^{\Delta2-145}$ cells, suggesting that the distal NSD plays little role in the temporal pattern of origin firing (Fig. 1A, profile 2). Thus, the inhibitory domain of NSD contributes to the repression of late origin firing when cells are under replication stress.

Distal NSD Functions to Restrict Replication Fork Progression. Although the distal NSD plays little role in the pattern of origin firing, we found that this domain has a strong influence on replication fork progression. In Fig. 1A, profile 2, the profile of $mcm4^{\Delta2-145}$ that lacks the distal NSD segment is plotted in red above the wild-type profile (shown in blue). It is evident that, across the genome, the peaks from the $mcm4^{\Delta2-145}$ mutant spread out more than those from the wild-type cells. Where several adjacent origins fire (e.g., Fig. 1A, near the centromere), multiple peaks from this mutant merge with each other. The more spread-out peaks suggest faster DNA synthesis from origins and thus faster-moving replication forks. In contrast, the peaks from cells lacking the proximal NSD segment ($mcm4^{\Delta74-174}$) are more restricted in fork progression overall than those in wild-type cells; computational analyses show an evident, although subtle, difference (Fig. 1 B and C). Consistent with a slower fork progression in the $mcm4^{\Delta74-174}$ mutant, we also observed in the time course experiment that the peak widths from 90–180 min change less in this mutant than in the wild type (Fig. S3). Furthermore, removal of the remaining distal NSD segment from $mcm4^{\Delta74-174}$ (e.g., as in $mcm4^{\Delta2-174}$) results in more fork progression than in $mcm4^{\Delta74-174}$ (Fig. 1A, profile 5, and Fig. 1B). Nevertheless, late origins fire efficiently

Table 1. Peak width of sites of initiation of DNA replication

Sample description	Mean peak width ± error in kb (number of peaks recorded)		
	Experiment 1	Experiment 2	Experiment 3
MCM4	11.1 ± 1.4 (114)	10.8 ± 1.6 (100)	9.7 ± 1.5 (106)
$mcm4^{\Delta2-145}$	—	19.2 ± 7.1 (44)	19.1 ± 5.3 (39)
$mcm4^{\Delta2-174}$	11 ± 2.4 (163)	11.3 ± 2 (167)	11.1 ± 1.5 (164)
$mcm4^{\Delta74-174}$	8.2 ± 0.7 (191)	8.2 ± 1 (169)	—
$mcm4^{\Delta74-174,\ 4(SP\rightarrow AP)}$	—	14.7 ± 2.4 (85)	—
$mcm4^{\Delta74-174,\ 4(SP\rightarrow DP)}$	—	10.1 ± 1.4 (117)	—
$mcm4^{5(SP\rightarrow AP)}$	—	18.7 ± 4.1 (42)	16.2 ± 4.1 (51)
$mcm4^{5(SP\rightarrow DP)}$	—	—	13.2 ± 1.4 (67)

Error stated uncertainties indicate 95% confidence interval.
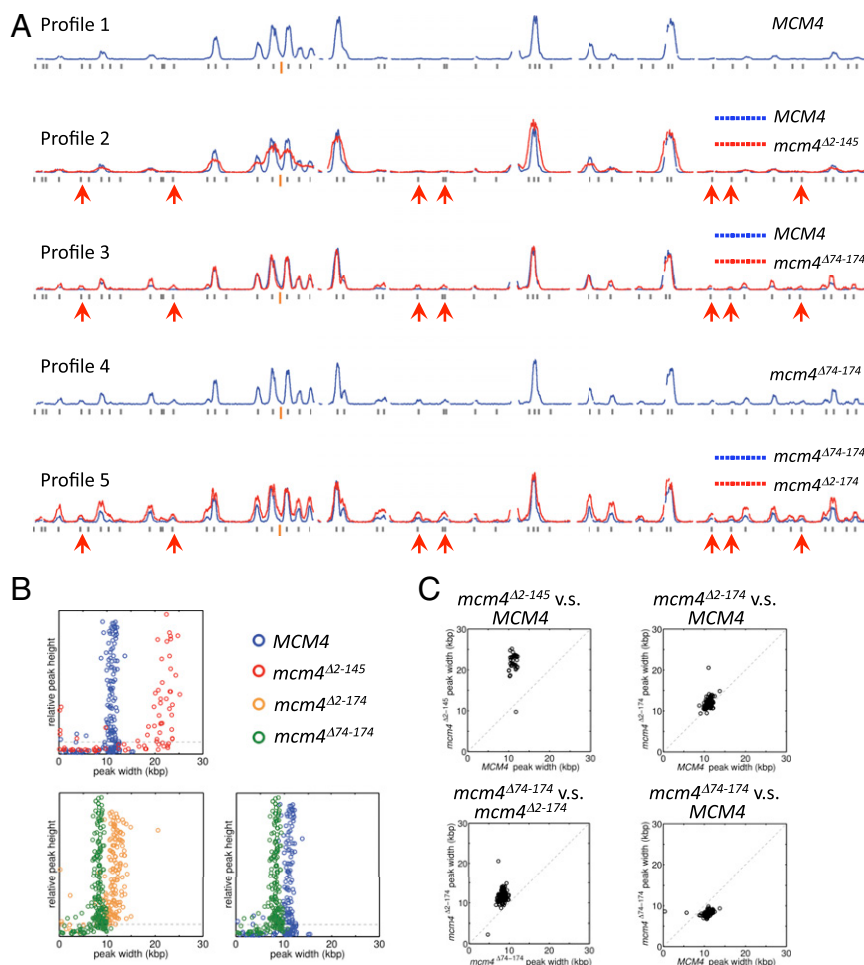
Fig. 1. Replication profile analyses of wild-type cells and mcm4 NSD mutants reveal patterns of origin activation and replication fork progression. YS2571, YS2574, YS2585, and YS2758 cells were synchronized in G1 phase and released into YPD containing 0.2 M HU and 0.5 mM EdU for 90 min. (*A*) Replication profiles of chromosome IV for wild-type cells and *mcm4* mutants with truncated NSD segments. Gray bars under the profiles indicate annotated replication origins according to the OriDB database. Orange bars indicate the location of centromeres. Red arrows indicate late origins that in HU are not active in wild-type cells but fire in the mutants lacking proximal NSD. Each profile was generated with mapped reads ranging from 0.69–1.68 million sequences. (*B*) Comparative distribution of the relative peak height versus peak width for origins from the replication profiles. Only peaks that colocalized with origins annotated in OriDB were recorded. (*C*) Pairwise comparisons of peak widths for individual origins in the mutant and the wild-type or indicated reference strains.
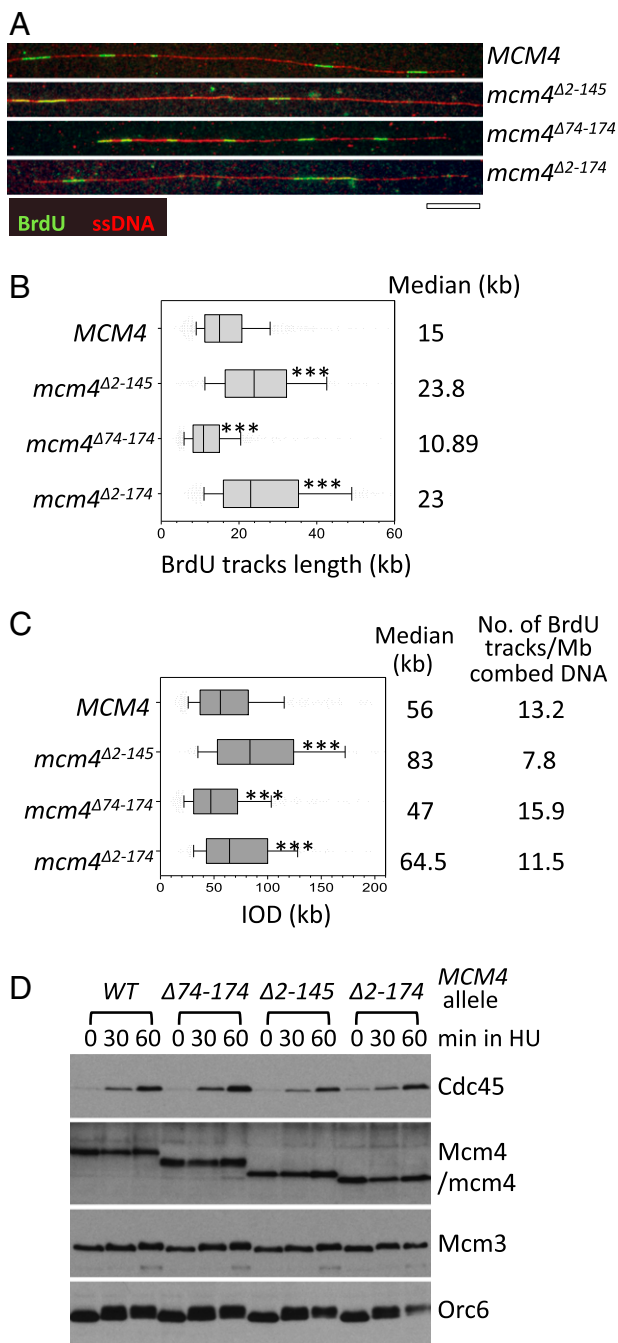
in the $mcm4^{\Delta 2-174}$ mutant. The difference in fork progression between $mcm4^{\Delta 2-174}$ and the wild type appears less pronounced, likely because multiple regulatory pathways are affected simultaneously in this mutant that lacks the entire NSD. Together, these data show that distal NSD segment plays an active role in restricting fork progression in HU.

Computational analysis of the peak widths clearly shows that forks progress further in $mcm4^{\Delta 2-145}$ (mean, 19.2 kb) than in the wild type (mean, 10.8 kb) (Fig. 1*B* and Table 1, Experiment 2). In contrast, forks progress less in the $mcm4^{\Delta 74-174}$ cells that lack the proximal NSD segment (mean, 8.2 kb). Pairwise comparisons of the fork progression from the same origins in mutants and wild-type cells (or the appropriate reference strain) (i.e., comparison of *ARS1* from one strain vs. *ARS1* from the other) revealed that the changes in fork progression are similar among all active origins, because the data cluster at a similar position on the plot (Fig. 1*C*). Together, these analyses clearly show that different parts of the NSD have different effects on replication fork progression.

Single-Molecule DNA Fiber Analyses Reveal an Important Role for the NSD in Replication Fork Progression. Analysis of the genome-wide replication profile reveals the average pattern of replication in a synchronized population of cells. To gain insight into the effect

of NSD mutants on DNA synthesis at the level of single origins, we used a molecular-combing technique (21). The same yeast strains used in the replication profile analysis were synchronized in G1 and released into HU and BrdU for 90 min. Chromosomal DNA from these cells was captured, stretched onto silanized coverslips, stained with anti-BrdU antibody, and visualized with fluorescent microscopy (Fig. 2*A*). The lengths of BrdU tracks were measured from many images similar to those shown here (Fig. 2*B*). The median track length for the wild type was 15 kb, versus 23.8 kb for $mcm4^{\Delta 2-145}$ (in which the distal NSD segment was deleted). This finding is consistent with the observation in whole-genome analyses that replication forks move further in $mcm4^{\Delta 2-145}$ than in the wild-type cells (Fig. 1). In contrast, the median track length for the $mcm4^{\Delta 74-174}$ cells was 10.9 kb, indicating slower fork progression in this mutant than in the wild type. Interestingly, removal of the entire NSD results in a median track length of 23 kb, similar to the track length when the distal NSD segment alone was removed. The median track length of the $mcm4^{\Delta 2-174}$ mutant in the DNA fiber analysis appears to be much longer than the mean fork progression computed in the DNA profile analysis. This discrepancy might result from the different limitations of these two completely different methods

A

BrdU   ssDNA

MCM4
mcm4^{Δ2-145}
mcm4^{Δ74-174}
mcm4^{Δ2-174}

B

Median (kb)

MCM4 — 15
mcm4^{Δ2-145} — *** — 23.8
mcm4^{Δ74-174} — *** — 10.89
mcm4^{Δ2-174} — *** — 23

BrdU tracks length (kb)

C

	Median (kb)	No. of BrdU tracks/Mb combed DNA
MCM4	56	13.2
mcm4^{Δ2-145} ***	83	7.8
mcm4^{Δ74-174} ***	47	15.9
mcm4^{Δ2-174} ***	64.5	11.5

IOD (kb)

D

WT   Δ74-174   Δ2-145   Δ2-174   MCM4 allele

0 30 60 0 30 60 0 30 60 0 30 60 min in HU

Cdc45

Mcm4/mcm4

Mcm3

Orc6

Fig. 2. Analyses of origin firing and replication fork progression in wild-type cells and *mcm4* mutants using DNA combing and chromatin fractionation. (*A–C*) Cells were synchronized in G1 phase and released into S phase in the presence of 0.2 M HU and 400 μg/mL of BrdU for 90 min. (*A*) Representative images of DNA fiber analyzed. BrdU is labeled with an anti-BrdU antibody (green), and DNA is counterstained with an antibody against ssDNA (red). (Scale bar: 50 kb.) (*B* and *C*) Box plots depict the length of BrdU-labeled tracks (track length) or the distance between two consecutive BrdU-labeled tracks (IOD). Boxes and whiskers indicate 25–75 and 10–90 percentiles, respectively. The statistical test is a Mann–Whitney test (nonparametric); *$P < 0.05$; **$P < 0.001$; ***$P \leq 0.0001$. (*B*) Distribution of BrdU track length. (*C*) Distribution of IOD. (*D*) Analysis of chromatin-bound proteins. Cells synchronized in G1 were released into 0.2 M HU and collected at the indicated time point. Chromatin-bound proteins were extracted from cells and analyzed by Western blot.

of analysis and the fact that the phenotype for this mutant is more complex by nature because it lacks both distal and proximal

NSDs that would exert opposing functions. Nevertheless, both analyses support the idea that the distal NSD segment plays an important role in controlling replication fork progression.

Proximal and Distal NSD Segments Have Opposing Effects on the Efficiency of Origin Firing in HU. DNA fiber analysis also allows measurement of the interorigin distance (IOD), which reveals the density of activated origins (Fig. 2*C*). We calculated the number of BrdU tracks per megabase of combed DNA, which indicates the overall efficiency of origin firing. The median IOD is shorter in for *mcm4*^{Δ74–174} cells [47 kilobases (kb)] than in wild-type cells (56 kb), suggesting more origins fire in the absence of the proximal NSD segment (Fig. 2*C*). Consistently, the number of BrdU tracks per megabase of DNA for *mcm4*^{Δ74–174} and for wild-type cells were 15.9 and 13.2, respectively, supporting the idea that *mcm4*^{Δ74–174} cells fire more efficiently than the wild-type cells, most likely because the ability of *mcm4*^{Δ74–174} cells to fire late origins in the presence of HU (Fig. 1*A*). Similarly, the median IOD for *mcm4*^{Δ2–174} cells was 64.5 kb, significantly shorter than the 83-kb median IOD for *mcm4*^{Δ2–145} cells, which possesses a small portion of the proximal NSD segment and do not fire late origins in HU (Fig. 1*A* and Fig. 2*C*). DNA fiber analysis also showed that removal of the distal NSD segment results in greater IOD and fewer BrdU tracks per megabase of DNA (Fig. 2*C*; compare the *mcm4*^{Δ2–145} mutant with the wild type and compare the *mcm4*^{Δ2–174} mutant with the *mcm4*^{Δ74–174} mutant). These results suggest that the distal NSD segment is important for efficient origin firing and that the proximal NSD segment controls the temporal pattern of origin activation by restricting origin firing in HU.

We also examined loading of the helicase-associated protein Cdc45 onto chromatin, a hallmark for origin activation (22). Cells were synchronized in G1, released into HU, and collected after 30 or 60 min. Chromatin-bound proteins were extracted from these samples and analyzed (Fig. 2*D* and Fig. S4). A slight increase in chromatin-bound Cdc45 in the *mcm4*^{Δ74–174} mutant, and a decrease in Cdc45 loading in the *mcm4*^{Δ2–145} mutant, both compared with wild type, was consistent with the idea that the proximal NSD functions to inhibit origin firing and that the distal NSD contributes positively to the same process. The *mcm4*^{Δ2–174} mutant, which lacks both proximal and distal NSD, has less Cdc45 on S-phase chromatin than the *mcm4*^{Δ74–174} mutant and has more than the *mcm4*^{Δ2–145} mutant. However, we consistently observed a subtle increase in Cdc45 on the G1 chromatin in this mutant. Nevertheless, the G1-to-S progression appears identical among all the strains in this experiment, as shown by the pattern of Orc6 phosphorylation, a marker for S-CDK activity (Fig. 2*D*, *Bottom Lane*). Together with the DNA fiber analyses, this chromatin fractionation experiment suggests that the proximal and distal NSD execute opposing effects on the efficiency of origin firing in HU.

Differential Effects of the Distal and Proximal NSDs on Checkpoint Signaling. Under replication stress and DNA-damaging conditions, the checkpoint-signaling pathway becomes activated and triggers several downstream responses, which include preventing late origin firing and inducing dNTP synthesis by RNR (Fig. 3*A*) (23–25). Although the *mcm4*^{Δ74–174} mutant fires late origins in HU (Fig. 1*A*), our previous study showed that this mutant is proficient in checkpoint activation (3). To gain a better picture of the checkpoint signaling in the NSD mutants, we conducted a comprehensive investigation of checkpoint responses in the wild type and various NSD mutants. Cells were synchronized in G1, released into HU, and collected at different time points. Protein extracts from these cells were analyzed by Western blot (Fig. 3 *B–D*). The checkpoint response indeed is more robust in the *mcm4*^{Δ74–174} cells than in the wild type, as revealed by higher levels of hyperphosphorylated Rad53 (the yeast Chk2 homolog) and
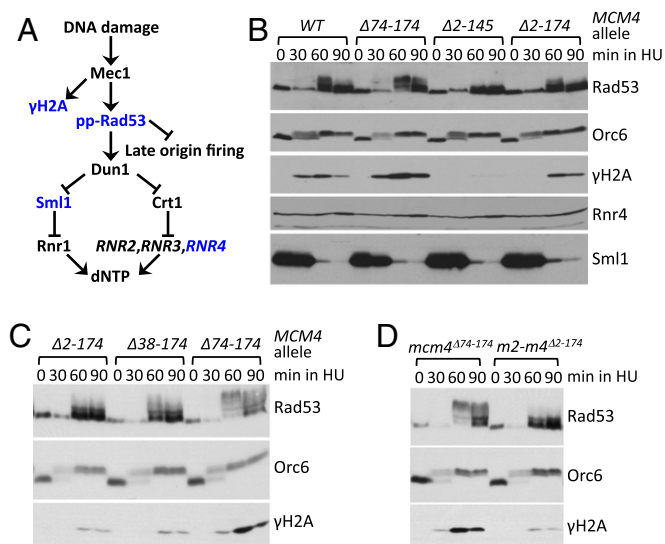
Fig. 3. NSD has various effects on checkpoint signaling. (A) Summary of the DNA damage checkpoint-signaling pathway. (B–D) Cells from the indicated strains were synchronized in G1, released into 0.2 M HU, and collected at the indicated time points. Protein samples were prepared using TCA extraction and were analyzed by Western blot. Yeast cells YS2534, YS2754, and YS2261 were used in C, and YS2261 and YS2263 ($m2\text{-}m4^{\Delta2\text{-}174}$ = $mcm2^{1\text{-}200}\text{-}mcm4^{\Delta2\text{-}174}$) were used in D.

naling directly downstream of Mec1, such as Rad53 hyperphosphorylation and H2A phosphorylation, are reduced or absent.
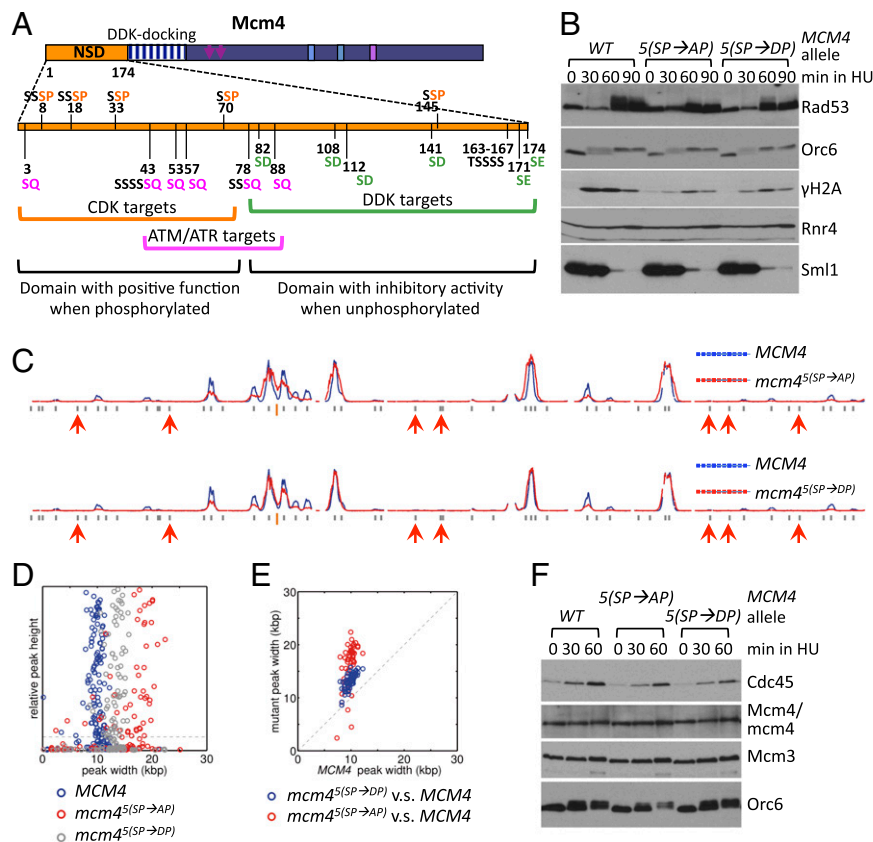
Phosphorylation of Serine-Proline Sites Within the Distal NSD Is Important for its Function in the Checkpoint Response and Replication Fork Progression. Although the NSD is structurally disordered and partly redundant within its subregions for cell growth, it appears to be organized in such way that the phospho-acceptor sites with signatures for particular types of kinases tend to cluster close to each other (Fig. 4A). For example, the serine-proline (SP) sites, which are targeted by CDK (16), are mostly found within the distal NSD segment. The SP sites in human Mcm4 also are concentrated within its distal NSD. Similarly, the serine-glutamine (SQ) sites, targeted by ATM/ATR, are concentrated mostly near the center of the NSD. Further, the serine-aspartic acid (SD)/serine-glutamic acid (SE) sites, preferred sites for DDK, are found mostly within the proximal NSD segment. Because the SP sites that are targeted by CDK lie within the distal NSD and might impact the function of this domain, we mutated the phospho-acceptors at all five SP sites into alanine (A) [5(SP→AP)] or phospho-mimetic aspartic acid (D) [5(SP→DP)] residues. The $mcm4^{5(SP\rightarrow AP)}$ mutant exhibited reduced phosphorylation of Rad53 and H2A under replication stress induced by HU [Fig. 4B, 5(SP→AP)], indicating limited checkpoint signaling. However, other Rad53-dependent responses, such as Sml1 degradation and induction of Rnr4, were normal, as they were in NSD distal domain-deletion mutants (Fig. 3B). Mutation of these sites to phospho-mimetic aspartic acids (i.e., $mcm4^{5(SP\rightarrow DP)}$) did not restore the normal HU-induced phosphorylation of Rad53 and H2A [Fig. 4B, 5(SP→DP)].

As seen with deletion of the distal NSD segment ($mcm4^{\Delta2\text{-}145}$), the 5(SP→AP) mutant exhibits increased fork progression in DNA replication profiles (Fig. 4 C–E), with a mean peak width of 16.2 kb, compared with 9.7 kb for the wild type in the same experiment (Table 1). In the replication profile analysis, fork progression of the $mcm4^{5(SP\rightarrow DP)}$ mutant (mean peak width, 13.2 kb) is less than in the $mcm4^{5(SP\rightarrow AP)}$ mutant but still is greater than in the wild type. Thus, the CDK-targeted SP sites within the NSD are important for control of replication fork progression.

One of the five SP sites also resides in the proximal NSD, which opposes the effect of the distal NSD on origin firing, checkpoint response, and fork progression (Figs. 1–3). Thus, the results we observed in the $mcm4^{5(SP\rightarrow AP)}$ and $mcm4^{5(SP\rightarrow DP)}$ mutants might combine the effects of mutating two opposing subdomains. Therefore we deliberately deleted the proximal NSD domain and examined the effect of the remaining SP→AP and SP→AD mutants in this background ($mcm4^{\Delta74\text{-}174}$). In the absence of the proximal NSD, $mcm4^{\Delta74\text{-}174}$ cells exhibit a robust checkpoint response as indicated by hyperphosphorylation of Rad53 and H2A (Figs. 3 and 5A). However, the levels of Rad53 hyperphosphorylation and H2A phosphorylation in the $mcm4^{\Delta74\text{-}174,\ 4(SP\rightarrow AP)}$ cells are very low (Fig. 5A). In contrast, the hyperphosphorylation levels of Rad53 and γH2A in the $mcm4^{\Delta74\text{-}174,\ 4(SP\rightarrow DP)}$ cells are comparable to those in $mcm4^{\Delta74\text{-}174}$ cells. Thus, phosphorylation at the four SP sites in the distal NSD controls checkpoint signaling.

Analysis of replication profiles showed that, like the $mcm4^{\Delta74\text{-}174}$ mutant, the $mcm4^{\Delta74\text{-}174,\ 4(SP\rightarrow AP)}$ and $mcm4^{\Delta74\text{-}174,\ 4(SP\rightarrow DP)}$ mutants still fire late origins in HU (Fig. 5B), suggesting that SP sites at the distal NSD do not control late origin firing under this condition.

This result is consistent with our earlier finding that the distal NSD plays little role in the pattern of origin firing (Fig. 1A). In contrast, we found that forks progress further in the $mcm4^{\Delta74\text{-}174,\ 4(SP\rightarrow AP)}$ mutant than in the $mcm4^{\Delta74\text{-}174}$ mutant, but the rates of fork progression in the $mcm4^{\Delta74\text{-}174,\ 4(SP\rightarrow DP)}$ mu-

increased levels of γH2A (phosphorylation of histone H2A at S129 in yeast). Both Rad53 and H2A are direct targets of the Mec1 kinase, the yeast ATM/ATR kinase (26, 27). Thus, despite an elevated checkpoint response, $mcm4^{\Delta74\text{-}174}$ cells are able to fire late origins in HU, suggesting that the proximal NSD plays an important role in mediating the inhibition of late origin firing under replication stress. Furthermore, the Sml1 inhibitor of RNR activity is degraded, and Rnr4, the damage-induced RNR subunit, is increased; both findings are consistent with intact checkpoint signaling in the $mcm4^{\Delta74\text{-}174}$ mutant (Fig. 3B). In contrast, both Rad53 hyperphosphorylation and γH2A are greatly diminished in the $mcm4^{\Delta2\text{-}145}$ cells. The slowest-migrating form of Rad53 was not detectable, although certain faster-migrating, hypophosphorylated forms of Rad53 could still be detected. γH2A was barely detectable in this mutant. Interestingly, other aspects of checkpoint signaling, such as Sml1 degradation and Rnr4 induction, appear normal in the $mcm4^{\Delta2\text{-}145}$ mutant that lacks the distal NSD (Fig. 3B).

We next asked what happens to the hyperactive checkpoint signaling in $mcm4^{\Delta74\text{-}174}$, the strain that had no proximal NSD, when it loses the distal NSD as well. Removal of the distal NSD entirely ($mcm4^{\Delta2\text{-}174}$) or partially ($mcm4^{\Delta38\text{-}174}$) from the $mcm4^{\Delta74\text{-}174}$ mutant causes weakening of the checkpoint response, as monitored by phosphorylation of Rad53 and H2A (Fig. 3C). Previously, we had shown that the acidic N-terminal domain (NTD) of Mcm2, another subunit of the MCM complex, could replace the distal NSD to support cell growth and to bypass the requirement for DDK efficiently (3, 15). The Mcm2 NTD also can be phosphorylated by DDK (13, 28). However, this domain failed to restore the checkpoint activation level, as shown by the reduced level of Rad53 hyperphosphorylation and γH2A in the $m2\text{-}m4^{\Delta2\text{-}174}$ mutant (short form for $mcm2^{1\text{-}200}\text{-}mcm4^{\Delta2\text{-}174}$) as compared with the $mcm4^{\Delta74\text{-}174}$ mutant (Fig. 3D). Together, these results suggest that a specific feature of the distal NSD is important for a complete checkpoint response under replication stress. Specifically, in the absence of the distal NSD of Mcm4, checkpoint signaling is initiated and propagated normally to at least some of the downstream effectors to boost RNR activity and dNTP levels, but other aspects of checkpoint sig-

Fig. 4. Phosphorylation of SP sites within the NSD affects checkpoint signaling and replication fork progression. (*A*) The Mcm4 NSD contains clusters of phospho-acceptor sites for multiple kinases. Different colors are used to show the distinct cluster of target sites for each type of kinase. (*B*–*F*) Cells used in *B*–*F* are YS2571, YS2755, and YS2813. (*B*) Different aspects of checkpoint signaling were assessed by Western blotting as described in Fig. 3. (*C*–*E*) Whole-genome DNA replication profile analysis. (*C*) Replication profiles from chromosome IV. Each profile was generated with mapped reads ranging from 4.80–7.32 million reads. Red arrows indicate late origins as in Fig. 1*A*. Note that these origins, which are active in the wild-type cells, are not active in these mutants. (*D*) Distribution of width and relative height of peaks in the replication profiles. (*E*) Pairwise comparison of peak widths for individual origins. (*F*) Cells synchronized in G1 and released into 0.2 M HU were collected, and chromatin-bound proteins were extracted and analyzed as described in Fig. 2*D*.

tant are similar to those in the $mcm4^{\Delta74–174}$ mutant. Computational analysis of the replication profiles showed that the peak widths for the $mcm4^{\Delta74–174}$, $mcm4^{\Delta74–174, 4(SP\to AP)}$, and $mcm4^{\Delta74–174, 4(SP\to DP)}$ mutants are 8.2, 14.7, and 10.1 kb, respectively (Table 1). Consistent with the replication profile analysis, DNA combing showed that the $mcm4^{\Delta74–174, 4(SP\to AP)}$ mutant has a median BrdU track length of 22.5 kb, significantly longer than the 10.9 kb and 10.0 kb of the $mcm4^{\Delta74–174}$ mutant and the $mcm4^{\Delta74–174, 4(SP\to DP)}$ mutant, respectively (Fig. 5*E* and Fig. S5). Together, these results demonstrate that phosphorylation of SP sites in the distal NSD mediates control of both the checkpoint response and replication fork progression but does not participate in controlling the pattern of origin firing.

The Effect of SP Site Phosphorylation on the Efficiency of Origin Firing. Although the pattern of late origin firing is not affected by the phosphorylation of SP sites in the distal NSD, the efficiency of origin firing is affected. DNA fiber analysis showed the median IODs for the $mcm4^{\Delta74–174}$, $mcm4^{\Delta74–174, 4(SP\to AP)}$, and $mcm4^{\Delta74–174, 4(SP\to DP)}$ mutants were 47, 68, and 53 kb, respectively, and the number of tracks per megabase of DNA are 15.9, 10.1, and 12.8, respectively (Fig. 5*F*). However, the effect does not appear to be as strong as that seen with fork progression or checkpoint response. Furthermore, we found that Cdc45 loading on chromatin is decreased only slightly in both $mcm4^{\Delta74–174, 4(SP\to AP)}$ and $mcm4^{\Delta74–174, 4(SP\to DP)}$ mutants, as compared with the $mcm4^{\Delta74–174}$ mutant (Fig. 5*G*). We also saw a slight decrease of Cdc45 on

chromatin in both alanine and aspartic mutants in the full-length context (Fig. 4*F*).

Distal NSD and Its Phosphorylation Are Important for Cell Growth Under Replication Stress. We have shown previously that simultaneous removal of both the proximal and distal NSD segments from Mcm4, as in the case of $mcm4^{\Delta2–174}$, leads to cold sensitivity, lethality in HU, and moderate delay in S-phase progression and slow growth at 30 °C (15). However, removal of only a portion of the NSD did not cause obvious growth defects. Previous studies also found little defect in cells with all SP sites mutated when the mutation of SP sites was not combined with additional mutations in other replication proteins (16). Thus, the NSD is dispensable when cells are grown under standard laboratory conditions (i.e., in rich medium at 30 °C). However, it is possible that the NSD evolved to allow cells to deal with stress conditions and to prevent genomic instability. In the presence of HU, which depletes dNTP pools and results in replication stress, cells lacking the distal NSD (i.e., $mcm4^{\Delta2–174}$ and $mcm4^{\Delta2–145}$ cells) do not grow or grow poorly (Fig. 6). In contrast, cells lacking only the proximal NSD ($mcm4^{\Delta74–174}$ cells) are able, like wild-type cells, to grow in HU. Cells in which he serine in SP sites has been changed to alanine within the NSD [e.g., $mcm4^{5(SP\to AP)}$ and $mcm4^{\Delta74–174, 4(SP\to AP)}$ cells] grow poorly in HU, although not as poorly as the mutant lacking the entire distal NSD. Importantly, mutation of these same sites to the phopho-mimetic aspartic acid residues [in $mcm4^{5(SP\to DP)}$ and $mcm4^{\Delta74–174, 4(SP\to DP)}$ cells]
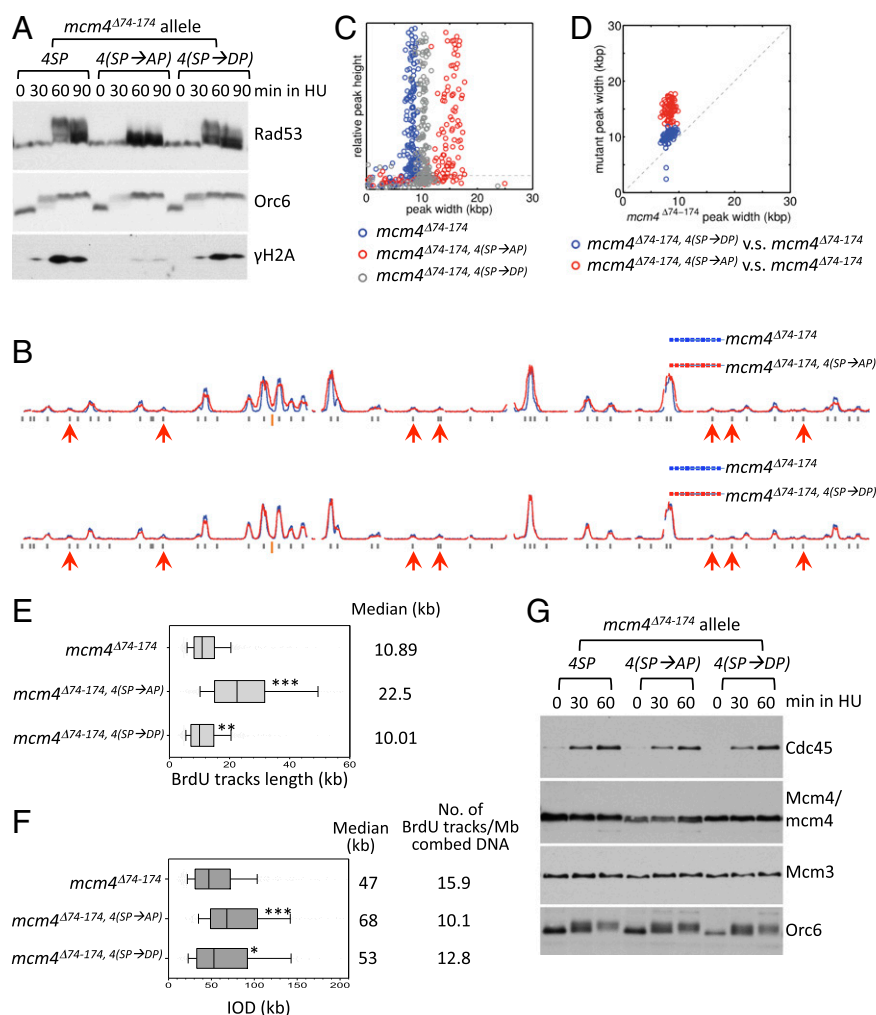
Fig. 5. Phosphorylation of SP sites within the distal NSD affects replication fork progression and checkpoint signaling. Yeast cells YS2574, YS2761, and YS2764 were used for the analyses in this figure. (*A*) Synchronized cells were collected, and various aspects of checkpoint signaling were analyzed as described in Fig. 3. (*B–D*) Whole-genome DNA replication profile analyses. Each profile was generated with reads ranging from 0.69–1.30 million reads. (*B*) Replication profiles from chromosome IV. Red arrows indicate late origins as in Fig. 1*A*. Note that late origins fire in all these mutants, which lack proximal NSD. (*C*) Distribution of width and relative height of peaks from the replication profiles. (*D*) Pairwise comparison of peak widths for individual origins. (*E* and *F*) DNA fiber analysis. (*E*) Distribution of BrdU track lengths. The statistical test is a Mann–Whitney test (nonparametric); *P < 0.05; **P < 0.001; ***P ≤ 0.0001. (*F*) Distribution of IOD. (*G*) Cells synchronized in G1 and released into 0.2 M HU were collected, and chromatin-bound proteins were extracted and analyzed as described in Fig. 2*D*.

allows growth in HU similar to that of wild type. Thus, the distal NSD segment plays an important role in cell growth under replication stress in a phosphorylation-dependent manner.

Discussion

Eukaryotic cells fire many origins during S phase with a distinct, spatial, and temporal pattern that often correlates with transcription activity and chromatin structures (29, 30). The timing pattern is influenced by chromosomal position and organization and by transacting factors. In this study, we developed a protocol to generate comprehensive and reproducible profiles of DNA replication patterns across the entire genome. Using simple computational analyses of these replication profiles, we assessed both origin utilization and replication fork progression from individual origins. DNA fiber analysis on single DNA molecules provides a complementary view, because the whole-genome profiles reflect the average patterns of DNA replication from a large number of cells. The two sets of data are congruent.

This and our previous studies (3, 15) have allowed us to attribute distinct functions within the N terminus of Mcm4 to the

proximal and distal NSDs (Fig. 7). We found that the proximal and distal NSDs overlap extensively in primary amino acid sequences, as is consistent with the property of a structurally disordered domain being multifunctional. Previously, we defined the proximal NSD (amino acids 74–174) as the domain whose removal is necessary for bypassing the essential regulation of DDK (3). Smaller deletions of only residues 146–174 or residues 98–174, are not sufficient to bypass DDK. In contrast, we found that a small portion of the proximal NSD (amino acids 146–174) encompasses the minimal domain that is sufficient to confer its inhibitory function that can be mitigated by DDK. Here, we further define the distal NSD (amino acids 2–145) as the domain whose removal is necessary to abolish the distal NSD functions in controlling fork progression and checkpoint responses. Deletion of only amino acids 2–74 was not sufficient to eliminate the function of the distal NSD. However, a smaller distal NSD domain comprising amino acids 2–74 is sufficient to confer the function of distal NSD and its regulation by CDK, as demonstrated using the set of mutants with deletion of residues 74–174
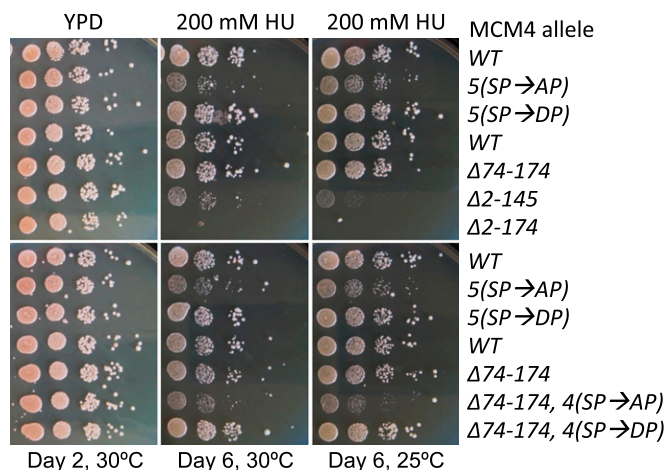
Fig. 6. NSD and its phosphorylation state play an important role in cell growth under replication stress. Shown are the results of serial 10-fold dilution of 10⁴ wild-type or NSD mutant cells on YPD or YPD + 0.2 M HU at the indicated temperature for the indicated number of days.

(Fig. 5). The diagram in Fig. 7 summarizes the functional domains within the Mcm4 NSD.

In this study we show that deletion of the proximal NSD causes late origins to fire, albeit inefficiently, in the presence of HU, despite a robust checkpoint response that normally should prevent late origin firing (23). The activation of late firing origins in HU in the absence of the Mcm4 proximal NSD might be anticipated because of the elimination of its initiation inhibitory activity (3). In yeast, DNA damage activates Mec1 kinase, which in turn activates Rad53 kinase to phosphorylate and inhibit the activities of Sld3 and Dbf4, thereby preventing late origin firing (11, 12). Because DDK targets the proximal NSD of Mcm4, inhibition of DDK by the checkpoint signaling has no consequence in the absence of this domain. The increased firing from late origins may contribute to the increased checkpoint activity in this mutant. That the late origins in this mutant fire at all indicates that the initiation-inhibiting activity of the proximal NSD mediates checkpoint signaling to block late origin firing. However, the extent of late origin firing is limited in its absence, likely because the other target of Rad53, Sld3, still is inhibited and thus prevents robust firing of late origins.

The distal segment of the Mcm4 NSD does not affect the overall temporal pattern of origin firing in HU. However, it is needed for efficient firing. The level of chromatin-bound Cdc45 is lower in the mutants than in the wild-type cells. The number of BrdU tracks per megabase of combed DNA decreases even more dramatically. However, we suggest that DNA fiber analysis might underestimate the efficiency of origin firing in this mutant, because some of the long track might result from fusion of adjacent tracks. Indeed merging of many adjacent replicons was observed in the whole-genome profile of *mcm4*^Δ2–145^, particularly near centromeres (Fig. 1A). Interestingly, when the entire NSD is removed (i.e., in *mcm4*^Δ2–174^ cells), late origin firing still is apparent, and the overall firing rate is higher than in the *mcm4*^Δ2–145^ mutant (although still lower than in the wild-type cells). We suggest that this phenotype is caused by the combined effects of the removal of both the distal and proximal NSD segments. To address specifically the role of the distal NSD in origin firing efficiency, we compared *mcm4*^Δ2–174^ and *mcm4*^Δ74–174^ cells. The data suggest that the distal NSD contributes to the efficient firing of early origins in HU. Thus, our data suggest that the NSD has a complex in the control of origin firing, with the distal NSD being important for efficient firing of early origins and the proximal NSD mediating the inhibition of origin firing.

The Mcm4 NSD also plays an important role in controlling DNA replication fork progression in a phosphorylation-dependent manner. Removal of the proximal NSD segment that is targeted by DDK results in a consistent decrease in fork progression. In contrast, deletion of the distal segment of the NSD (as in the *mcm4*^Δ2–145^ mutant) or mutation of the known CDK sites in this segment causes extensive replication fork progression from all origins across the genome. Interestingly, most of the SP sites are clustered within the distal segment of the Mcm4 NSD and are known to be targeted by CDK (16). Thus, it is likely the effect we observed depends on CDK activity. However, this possibility does not preclude the involvement of other types of kinase, in particular MAP kinases, which often are activated by environmental stress and also target the SP sites (31).

Surprisingly, deletion of the Mcm4 NSD distal segment or mutation of the SP sites causes a defect in only some aspects of the checkpoint signaling pathway. In these mutants, Rad53 is hypophosphorylated, and H2A is not phosphorylated in the presence of HU. However, other aspects of checkpoint signaling are normal, including up-regulation of Rnr4 and Sml1 degradation, both of which contribute to increased RNR activity and higher dNTP levels. Thus, we suggest that the Mcm4 NSD influences checkpoint signaling only on specific effectors near the replication forks. We found that the Mec1/Ddc2 complex is associated with the MCM complex on chromatin throughout the cell-division cycle in wild-type cells and NSD mutants. Thus, the NSD does not tether the Mec1/Ddc2 complex to MCM. Rather, it might affect the activity of the Mec1 kinase toward a subset of its substrates, such as Rad53 and H2A.

For both distal and proximal segment deletion, the results revealed an interesting inverse correlation between checkpoint signaling and DNA replication fork progression, raising the possibility that one process controls the other. In addition to inhibiting late origin firing, checkpoint signaling is thought to play an important role in stabilizing the DNA replication intermediates at the forks. Thus it is tempting to speculate that the checkpoint slows down fork progression while stabilizing it. In *Drosophila*, Chk2 (the homolog of Rad53) interferes with the helicase activity by targeting multiple components of the CMG, including Mcm4, and inhibits the activity of the helicase complex (10). In human cells, HU induces hyperphosphorylation of Mcm4 involving the consecutive action of ATR-CHK1 and CDK2 kinases (7). It has been shown that CDK phosphorylation at the NTD of human Mcm4 inhibit the helicase activity of the Mcm4,6,7 complex (32). Interestingly, the CDK sites in human Mcm4 also are most concentrated at the distal portion of its
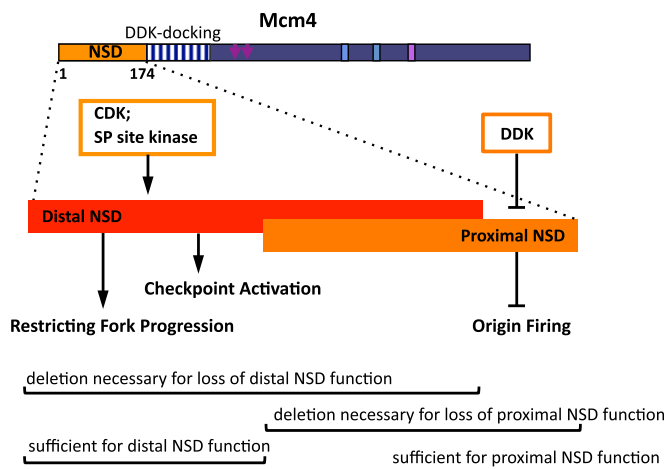
Fig. 7. Summary of functional domains within the Mcm4 NSD.

NTD. Thus, it is likely that phosphorylation of SP sites at distal NSD slows down fork progression under stress conditions by modulating the activity of the replicative helicase. The ability to slow down the replication fork may be important for cell viability under replication stress. Consistent with this idea, we found that mutants without the distal NSD or with SP sites mutated to alanine, which cannot be phosphorylated, exhibit a slow-growth phenotype in the presence of HU.

In addition to clusters of SP sites, the yeast NSD of Mcm4 also possesses a cluster of SQ sites (Fig. 4*A*). This cluster, which is targeted by Mec1, also may be important for the function of distal NSD. Consistent with this possibility, we found that the *mcm4*$^{\Delta 38-174}$ mutant, in which several SQ sites also have been removed, exhibits a weakened checkpoint response (Fig. 3*B*). We are investigating the role of these sites in regulating of the Mcm4 NSD function.

It has been shown that dNTP levels influence the rate of replication fork progression (33). However, because the pathway that leads to up-regulation of dNTP pools is not affected in the NSD mutants, NSD likely regulates fork progression by through alternative mechanisms, such as control of the replicative helicase. Another attractive possibility is the involvement of Mrc1, which is required for normal fork progression (34). Mrc1 interacts with MCM (4) and, under replication stress, forms a stable pausing complex with the replisome to facilitate repair (35). Moreover, Mrc1 is a target of Mec1 and facilitates phosphorylation of Rad53 under replication stress (36). Mrc1 also facilitates phosphorylation of chromatin-bound Mcm4 by Mec1 during S phase or in HU (13). Furthermore, Mrc1 interacts with Pol2 in a checkpoint-dependent manner, and it has been proposed that Mrc1 mediates DNA synthesis and unwinding at the replication fork (37). It remains to be resolved whether Mrc1 promotes or restricts fork progression. We suggest that the function of Mrc1 may be tightly linked to the NSD of Mcm4 and, similarly, may exert a more complex effect than simply blocking or promoting fork progression.

Control of spatial and temporal patterns of initiation and regulation of replication fork progression in response to the environment are important aspects in maintaining genome stability. Our studies reveal that the proximal and distal NSD segments in Mcm4 execute differential effects on many aspect of DNA replication, such as origin use, firing efficiency, replication fork progression, and checkpoint signaling. The ability of this domain to regulate a process both positively and negatively allows more subtle and sophisticated control in the face of changing environments. Our work suggests that cells modulate the pattern of replication in response to environmental conditions through regulation of the multifunctional NSD.

Materials and Methods

Yeast Strains and Methods. Yeast strains generated in this study were derived from W303-1a (*MATa ade2-1 can1-100 his3-11,15 leu2-3,112 trp1-1 ura3-1*) and are described in Table S1. A two-step gene-replacement method was used to replace the endogenous *MCM4* with *mcm4* mutants as described (3). All the yeast strains used for the whole-genome DNA replication profile

analyses and DNA fiber analyses have a copy of the BrdU-Inc cassette inserted into the *URA3* locus (17).

For G1 arrest, exponentially growing *bar1Δ* yeast cells (~10^7 cells/mL) were synchronized in G1 with 25 ng/mL of α-factor for 150 min at 30 °C. To release cells from G1 arrest, cells were collected by filtration and promptly washed twice on a filter (55-Plus Monitor filter unit, 0.45 μm, Millipore) using one culture volume of H$_2$O and then were resuspended in yeast extract/peptone/dextrose (YPD) medium containing 0.2 mg/mL pronase E (Sigma).

Protein Sample Preparation and Immunoblot Analysis. Trichloroacetic acid (TCA) extraction of yeast proteins was performed as previously described (3). For chromatin fractionation, chromatin pellets were prepared from ~5×10^8 yeast cells, and chromatin-bound proteins were released using DNase I using a procedure scaled down from a protocol described previously (15). For immunoblot analysis, protein samples were fractionated by SDS/PAGE and transferred to nitrocellulose membrane. Immunoblot analysis for Mcm3, Cdc45, and Orc6 was performed as described (3, 38). For detection of Mcm4, antibody Mcm4 (yC-19) (sc-6685; Santa Cruz Biotechnology, Inc.) was used at a 1:1,000 dilution. For analysis of Rad53, TCA-extracted yeast proteins were fractionated in 10% SDS/PAGE according to ref. 39. Rad53 (yC-19) antibody sc-6749 (Santa Cruz Biotechnology, Inc.) was used at a 1:1,000 dilution, and TBS + 0.1% Tween 20 was used for preparing blocking and washing solutions. Rabbit anti-S129 (catalog no. ab15083; Abcam) was used at a 1:1,000 dilution to detect γ-H2A. Rat antibodies YL1/2 were used at 1:2,500 to detect Rnr4, and rabbit anti-sml1 was used at 1:5,000 to detect Sml1.

Isolation and Preparation of DNA for Whole-Genome Replication Profile Analysis. The protocol is described in detail in *SI Materials and Methods*, *Isolation and Preparation of DNA for Whole-Genome Replication Profile Analysis*. Briefly, yeast cells were synchronized in G1 with α-factor and were released into medium containing 0.2 mg/mL pronase E, 0.2 M HU, and 0.5 mM EdU. At the indicated time points, cells were collected by centrifugation for preparation of genomic DNA. The genomic DNA was fragmented and then ligated to adaptors containing custom barcodes (Table S2). The barcoded EdU-genomic DNA then was biotinylated using the Click reaction and purified using Streptavidin T1 magnetic beads (Invitrogen). The purified, barcoded, biotinylated DNA was PCR-amplified for 14 cycles, quantified, pooled, and submitted for sequencing. Computational analyses of sequencing data are described in detail in *SI Materials and Methods*, *Computational Analyses of Sequencing Data*. DNA sequencing data were submitted to the Sequence Read Archive database [www.ncbi.nlm.nih.gov/sra (accession no. SRP040450)].

DNA Fiber Analysis. DNA combing was performed as previously described (21). Cells were synchronized in G1 with α-factor at 30 °C and released with 50 μg/mL of pronase into S phase in the presence of 0.2 M HU and 400 μg/mL BrdU for 90 min. Box plots depict the length of BrdU-labeled tracks (track length) or the distance between two consecutive BrdU-labeled tracks (IOD). Boxes and whiskers indicate 25–75 and 10–90 percentiles, respectively.

1. Tanaka S, et al. (2007) CDK-dependent phosphorylation of Sld2 and Sld3 initiates DNA replication in budding yeast. *Nature* 445(7125):328–332.
2. Zegerman P, Diffley JF (2007) Phosphorylation of Sld2 and Sld3 by cyclin-dependent kinases promotes DNA replication in budding yeast. *Nature* 445(7125):281–285.
3. Sheu YJ, Stillman B (2010) The Dbf4-Cdc7 kinase promotes S phase by alleviating an inhibitory activity in Mcm4. *Nature* 463(7277):113–117.
4. Gambus A, et al. (2006) GINS maintains association of Cdc45 with MCM in replisome progression complexes at eukaryotic DNA replication forks. *Nat Cell Biol* 8(4):358–366.
5. Moyer SE, Lewis PW, Botchan MR (2006) Isolation of the Cdc45/Mcm2-7/GINS (CMG) complex, a candidate for the eukaryotic DNA replication fork helicase. *Proc Natl Acad Sci USA* 103(27):10236–10241.
6. Pacek M, Tutter AV, Kubota Y, Takisawa H, Walter JC (2006) Localization of MCM2-7, Cdc45, and GINS to the site of DNA unwinding during eukaryotic DNA replication. *Mol Cell* 21(4):581–587.

7. Ishimi Y, Komamura-Kohno Y, Kwon HJ, Yamada K, Nakanishi M (2003) Identification of MCM4 as a target of the DNA replication block checkpoint system. *J Biol Chem* 278(27):24644–24650.
8. Matsuoka S, et al. (2007) ATM and ATR substrate analysis reveals extensive protein networks responsive to DNA damage. *Science* 316(5828):1160–1166.
9. De Piccoli G, et al. (2012) Replisome stability at defective DNA replication forks is independent of S phase checkpoint kinases. *Mol Cell* 45(5):696–704.
10. Ilves I, Tamberg N, Botchan MR (2012) Checkpoint kinase 2 (Chk2) inhibits the activity of the Cdc45/MCM2-7/GINS (CMG) replicative helicase complex. *Proc Natl Acad Sci USA* 109(33):13163–13170.
11. Zegerman P, Diffley JF (2010) Checkpoint-dependent inhibition of DNA replication initiation by Sld3 and Dbf4 phosphorylation. *Nature* 467(7314):474–478.
12. Lopez-Mosqueda J, et al. (2010) Damage-induced phosphorylation of Sld3 is important to block late origin firing. *Nature* 467(7314):479–483.

13. Randell JC, et al. (2010) Mec1 is one of multiple kinases that prime the Mcm2-7 helicase for phosphorylation by Cdc7. *Mol Cell* 40(3):353–363.
14. Duch A, et al. (2013) Coordinated control of replication and transcription by a SAPK protects genomic integrity. *Nature* 493(7430):116–119.
15. Sheu YJ, Stillman B (2006) Cdc7-Dbf4 phosphorylates MCM proteins via a docking site-mediated mechanism to promote S phase progression. *Mol Cell* 24(1):101–113.
16. Devault A, Gueydon E, Schwob E (2008) Interplay between S-cyclin-dependent kinase and Dbf4-dependent kinase in controlling DNA replication through phosphorylation of yeast Mcm4 N-terminal domain. *Mol Biol Cell* 19(5):2267–2277.
17. Viggiani CJ, Aparicio OM (2006) New vectors for simplified construction of BrdU-Incorporating strains of Saccharomyces cerevisiae. *Yeast* 23(14-15):1045–1051.
18. Salic A, Mitchison TJ (2008) A chemical method for fast and sensitive detection of DNA synthesis in vivo. *Proc Natl Acad Sci USA* 105(7):2415–2420.
19. Nieduszynski CA, Hiraga S, Ak P, Benham CJ, Donaldson AD (2007) OriDB: A DNA replication origin database. *Nucleic Acids Res* 35(Database issue):D40–D46.
20. Alvino GM, et al. (2007) Replication in hydroxyurea: It's a matter of time. *Mol Cell Biol* 27(18):6396–6406.
21. Bianco JN, et al. (2012) Analysis of DNA replication profiles in budding yeast and mammalian cells using DNA combing. *Methods* 57(2):149–157.
22. Zou L, Stillman B (1998) Formation of a preinitiation complex by S-phase cyclin CDK-dependent loading of Cdc45p onto chromatin. *Science* 280(5363):593–596.
23. Santocanale C, Diffley JF (1998) A Mec1- and Rad53-dependent checkpoint controls late-firing origins of DNA replication. *Nature* 395(6702):615–618.
24. Zhao X, Chabes A, Domkin V, Thelander L, Rothstein R (2001) The ribonucleotide reductase inhibitor Sml1 is a new target of the Mec1/Rad53 kinase cascade during growth and in response to DNA damage. *EMBO J* 20(13):3544–3553.
25. Elledge SJ, Zhou Z, Allen JB, Navas TA (1993) DNA damage and cell cycle regulation of ribonucleotide reductase. *BioEssays* 15(5):333–339.
26. Cobb JA, et al. (2005) Replisome instability, fork collapse, and gross chromosomal rearrangements arise synergistically from Mec1 kinase and RecQ helicase mutations. *Genes Dev* 19(24):3055–3069.
27. Pellicioli A, et al. (1999) Activation of Rad53 kinase in response to DNA damage and its effect in modulating phosphorylation of the lagging strand DNA polymerase. *EMBO J* 18(22):6561–6572.
28. Stead BE, Brandl CJ, Davey MJ (2011) Phosphorylation of Mcm2 modulates Mcm2-7 activity and affects the cell's response to DNA damage. *Nucleic Acids Res* 39(16):6998–7008.
29. Rhind N, Gilbert DM (2013) DNA replication timing. *Cold Spring Harb Perspect Biol* 5(8):a010132.
30. Aparicio OM (2013) Location, location, location: It's all in the timing for replication origins. *Genes Dev* 27(2):117–128.
31. Mok J, et al. (2010) Deciphering protein kinase specificity through large-scale analysis of yeast phosphorylation site motifs. *Sci Signal* 3(109):ra12.
32. Ishimi Y, Komamura-Kohno Y (2001) Phosphorylation of Mcm4 at specific sites by cyclin-dependent kinase leads to loss of Mcm4,6,7 helicase activity. *J Biol Chem* 276(37):34428–34433.
33. Poli J, et al. (2012) dNTP pools determine fork progression and origin usage under replication stress. *EMBO J* 31(4):883–894.
34. Tourrière H, Versini G, Cordón-Preciado V, Alabert C, Pasero P (2005) Mrc1 and Tof1 promote replication fork progression and recovery independently of Rad53. *Mol Cell* 19(5):699–706.
35. Katou Y, et al. (2003) S-phase checkpoint proteins Tof1 and Mrc1 form a stable replication-pausing complex. *Nature* 424(6952):1078–1083.
36. Alcasabas AA, et al. (2001) Mrc1 transduces signals of DNA replication stress to activate Rad53. *Nat Cell Biol* 3(11):958–965.
37. Lou H, et al. (2008) Mrc1 and DNA polymerase epsilon function together in linking DNA replication and the S phase checkpoint. *Mol Cell* 32(1):106–117.
38. Weinreich M, Stillman B (1999) Cdc7p-Dbf4p kinase binds to chromatin during S phase and is regulated by both the APC and the RAD53 checkpoint pathway. *EMBO J* 18(19):5334–5346.
39. Puddu F, Piergiovanni G, Plevani P, Muzi-Falconi M (2011) Sensing of replication stress and Mec1 activation act through two independent pathways involving the 9-1-1 complex and DNA polymerase ε. *PLoS Genet* 7(3):e1002022.